IEEE Access
Multidisciplinary | Rapid Review | Open Access Journal

Received March 16, 2020, accepted March 27, 2020, date of publication March 31, 2020, date of current version April 16, 2020.

Digital Object Identifier 10.1109/ACCESS.2020.2984487

ISAR Imaging of Non-Uniform Rotating Targets Based on Optimized Matching Fourier Transform

LEI ZUO AND BINBIN WANG
College of Electronic Engineering, Naval University of Engineering, Wuhan 430033, China
Corresponding author: Binbin Wang (bbwang2016@126.com)

This work was supported by the China Postdoctoral Science Foundation under Grant 2016M603007.

ABSTRACT Uniformly accelerated rotation of maneuvering targets can lead to quadratic phase terms, after translational motion compensation, which causes the cross-range signal in a certain range cell to be multicomponent linear frequency modulated (LFM) signals. Due to the time-varying Doppler frequencies of scatterers, ISAR image obtained by the conventional range-Doppler (RD) algorithm is blurred severely. To solve this problem, a new imaging method based on optimized matching Fourier transform (MFT) is proposed in this paper. In the new method, the equivalent rotation of targets is described by the rotation ratio (RR) which is the same for all scatterers on the target. The quadratic phase components caused by target's angular acceleration can be compensated by MFT, as soon as the RR is obtained. The estimation of RR is achieved according to the optimal imaging result with the image entropy as the cost function. As a result, the blurring of the ISAR image is eliminated effectively and a well-focused image is got. From the experimental results using simulated data, it can be concluded that the proposed method based on optimized MFT is effective in ISAR imaging of non-uniform rotating targets in terms of image quality and computational efficiency.

INDEX TERMS Inverse synthetic aperture radar (ISAR), non-uniform rotating targets imaging, matching Fourier transform, gradient descent optimization.

I. INTRODUCTION

Inverse synthetic aperture radar (ISAR) imaging is believed to have the ability for high-resolution imaging and recognition [1]–[8], and plays an important role in civil and military fields. In general, after range compression, translational motion compensation (TMC), which includes range alignment and phase adjustment, is carried out. Then, high-quality ISAR images can be obtained by range-Doppler (RD) algorithm [9], [10]. To satisfy the condition that the scatterer's Doppler frequency is constant during the coherent processing interval (CPI) and can only apply for ISAR imaging of targets with uniform velocity. However, for targets with complex motion, the Doppler frequency of each scatterer is time-varying, which causes the ISAR images obtained by the RD algorithm smeared severely. ISAR imaging of non-uniform rotating targets have gained traction in the research community and many algorithms [11], [12] have been proposed. These algorithms can be divided into two categories: parametric and nonparametric approaches.

The associate editor coordinating the review of this manuscript and approving it for publication was Yong Wang.

As for the parametric approach, the received radar echo in a range cell is modelled as multicomponent linear frequency modulated (LFM) signals or cubic phase signals. The well-focused instantaneous ISAR image can be reconstructed by estimating the parameters of the signals. For the low maneuvering targets, such as satellites and airplanes, the motion can be regarded as uniformly accelerated rotation after TMC, and each scatterer can be characterized by an LFM signal. Several successful estimation algorithms for LFM signal have been proposed, which contain the stretch keystone-Wigner transform [13], the fractional Fourier transform [14] and Lv's distribution (LVD) [15], etc. However, this approach is computationally extensive and inefficient due to the demand for estimating the parameters of each LFM component.

Nonparametric approach is built on joint time-frequency representations (JTFR) [16]–[19], which is an substitute of Fourier transform in the cross-range focusing process The most widely used JTFR encompasses the short-time Fourier transform (STFT), the Wigner-Ville distribution (WVD) [16] and the smoothed pseudo-WVD (SPWVD) [17] et al. Due to the window function, the STFT usually has a low resolution.

This work is licensed under a Creative Commons Attribution 4.0 License. For more information, see https://creativecommons.org/licenses/by/4.0/

The others have the virtue of computational efficiency; however, a compromise must be made between the time-frequency resolution and the ability to suppress the cross-term interference.

In this paper, we focus on the imaging of non-uniform rotating targets and proposed a novel imaging method based on optimized MFT. After TMC, the rotation of the targets can be described by uniformly accelerated rotation model, and the cross-range signal in a certain range cell to be multi-component LFM signals. For targets with rigid body, the ratio of the chirp rate and centroid frequency of the LFM signals which is defined as rotation ratio (RR) are identical for all scatterers and only depends on target's rotation parameter. Once the RR is obtained, the quadratic phase components caused by target's acceleration can be compensated by MFT. Based on that, ISAR imaging of non-uniform rotating targets is converted into a parameter estimation problem. The coarse estimation of RR is obtained by LVD, and the accurate one is estimated according to the optimal imaging result by gradient descent method (GDM). As a result, the blurring of the image is eliminated effectively and a well-focused ISAR image is got under a reasonable computational cost.

The remainder of this paper is arranged as follows. The imaging signal model of non-uniform rotating targets is established in Section 2. The principles of the proposed imaging method are elaborated in Section 3. Section 4 validates the proposed method by simulations and the conclusion is provided in Section 5.

II. IMAGING SIGNAL MODEL OF NON-UNIFORM ROTATING TARGETS

Figure.1 shows the typical ISAR imaging geometry. The radar is located on the target plane along Y-axis, R_0 is the distance from the rotational center to the radar. (x_i, y_i) is the coordinates of the i-th scatterer on the target. After range compression and TMC, the cross-range signal in a certain range cell can be written as

$$s(t_m) = \sum_{i=1}^{Q} \sigma_i \exp\left\{-\frac{j4\pi}{\lambda}\left(x_i \sin\theta(t_m) + y_i \cos\theta(t_m)\right)\right\} \tag{1}$$

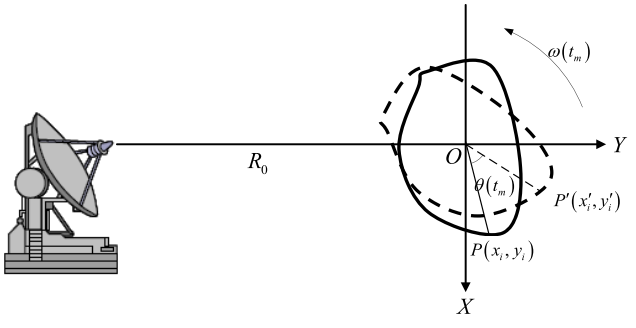

FIGURE 1. The geometry of ISAR imaging.

where Q is the number of scatterers in this range cell, σ_i is the reflection coefficient, λ is the wavelength and $\theta(t_m)$ is the instantaneous rotational angle of the target.

The Taylor expansion of the rotational angle can be expressed as follows:

$$\theta(t_m) = \omega t_m + \frac{1}{2}\alpha t_m^2 + \frac{1}{6}\beta t_m^3 + \ldots \tag{2}$$

where ω is the equivalent angular velocity, $\alpha$is the angular acceleration and β is the angular jerk.

For targets with uniform velocity, the target's rotational angle is expressed as $\theta(t_m) = \omega t_m$. In general, $\theta(t_m)$ is small during the CPI, so we have the following approximations:

$$\begin{aligned} \sin\theta(t_m) &\approx \theta(t_m) = \omega t_m \\ \cos\theta(t_m) &\approx 1 \end{aligned} \tag{3}$$

Substituting (3) into (1) yields

$$s(t_m) = \sum_{i=1}^{Q} \sigma_i \exp\left\{-\frac{j4\pi}{\lambda}\left(x_i \omega t_m + y_i\right)\right\} \tag{4}$$

Obviously, the linear phase component in (4) corresponds to the cross-range position of the i-th scatterer.

The well-focused ISAR image can be obtained by performing FT with respect to t_m.

As for the non-uniform rotating target, the equivalent angular velocity is not constant and the rotational angle is $\theta(t_m) = \omega t_m + \frac{1}{2}\alpha t_m^2$. In this case, (1) turns into

$$\begin{aligned} s(t_m) &= \sum_{i=1}^{Q} \sigma_i \exp\left\{-\frac{j4\pi}{\lambda}\left(x_i \omega t_m + \frac{1}{2} x_i \alpha t_m^2 + y_i\right)\right\} \\ &= \sum_{i=1}^{Q} \sigma_i \exp\left(-j2\pi\left(f_i t_m + \frac{1}{2} k_i t_m^2\right)\right) \exp\left(-\frac{j4\pi y_i}{\lambda}\right) \end{aligned} \tag{5}$$

where $f_i = \frac{2x_i\omega}{\lambda}$, $k_i = \frac{2x_i\alpha}{\lambda}$. Equation (5) indicates that the cross-range signals are multicomponent LFM signal. The centroid frequency f_i and the chirp rate k_i depend on the scatterer's azimuth coordinate and rotation parameters. It is the quadratic phase term of LFM signals that cause the blurring of ISAR image, thus it must be compensated. Next, we focus on the compensation of the quadratic phase terms.

III. IMAGING METHOD BASED ON OPTIMIZED MFT

A. ALGORITHM DESCRIPTION

MFT [21], [22] is developed on the basis of FT and is widely-used in non-stationary signal processing. For a signal

$$f(t) = \sum a_i \exp(j\omega_i \phi(t)) \tag{6}$$

The MFT is defined as

$$F(\omega) = \int_0^T f(t) e^{j\omega\phi(t)} d\phi(t) \tag{7}$$

where $\phi(t)$ is the frequency modulation function. It can be seen from equation (6) and (7) that the spectrum of random modulated signal can be obtained by MFT.

Next, we define the RR as

$$K_{\alpha\omega} = \frac{k_i}{f_i} = \frac{\alpha}{\omega} \tag{8}$$

Obviously, $K_{\alpha\omega}$ is identical for all scatterers and only depends on target's rotation parameters: equivalent angular velocity ω and angular acceleration α.

Now, the equation (5) can be rewritten as Now, the equation (5) can be rewritten as

$$\begin{aligned} s(t_m) &= \sum_{i=1}^{Q} \sigma_i \exp\left\{-\frac{j4\pi}{\lambda}\left(x_i\omega t_m + \frac{1}{2}x_i\alpha t_m^2 + y_i\right)\right\} \\ &= \sum_{i=1}^{Q} \sigma_i \exp\left\{-j2\pi\left(f_i t_m + \frac{1}{2}k_i t_m^2\right)\right\} \exp\left(-\frac{j4\pi y_i}{\lambda}\right) \\ &= \sum_{i=1}^{Q} \sigma_i \exp\left\{-\frac{j4\pi}{\lambda}x_i\omega\left(t_m + \frac{1}{2}K_{\alpha\omega}t_m^2\right)\right\} \\ &\quad \times \exp\left(-\frac{j4\pi y_i}{\lambda}\right) \end{aligned} \tag{9}$$

We neglect $\sum_{i=1}^{Q} \sigma_i \exp\left(-\frac{j4\pi y_i}{\lambda}\right)$ which correspond to range position and denote $b_i = -\frac{j4\pi}{\lambda}x_i\omega$ and $\psi(t_m) = t_m + \frac{1}{2}K_{\alpha\omega}t_m^2$. Then (9) turns into

$$s(t_m) = \sum_{i=1}^{Q} \sigma_i \exp\left[jb_i\psi(t_m)\right] \tag{10}$$

It can be noticed that the equation (10) has the same form as (6) and $\psi(t_m)$ is monotonic bounded during the CPI. Thus, MFT can be utilized to accomplish cross-range compression.

B. COARSE ESTIMATION OF RR BASED ON LVD

The aforementioned analysis is based on an implicit assumption that the RR is already known. However, the assumption is invalid for noncooperative targets and the RR needs to be estimated in advance. Equation (5) indicates that the cross-range signals are multicomponent LFM signals, LVD can be applied to estimate the RR. For a continuous infinite-time multicomponent LFM signal

$$s(t_m) = \sum_{k=1}^{K} A_k \exp\left(j2\pi f_k t_m + j\pi k_k t_m^2\right) \tag{11}$$

The autocorrelation function is defined as

$$\begin{aligned} R_s^c(\tau, t_m) &= \sum_{k=1}^{K} s\left(t_m + \frac{\tau + a}{2}\right) s^*\left(t_m - \frac{\tau + a}{2}\right) \\ &= \sum_{k=1}^{K} A_k^2 \exp\left(j2\pi f_k(\tau + a)t_m + j2\pi k_k(\tau + a)t_m\right) \\ &\quad + \sum_{k=1}^{K-1}\sum_{l=k+1}^{K}\left[R_{sk,sl}^c(\tau, t_m) + R_{sl,sk}^c(\tau, t_m)\right] \end{aligned} \tag{12}$$

where $*$ denotes the complex conjugation, τ is the lag-time variable, a is the constant time-delay parameter, R_{sk}^c and $R_{sk,sl}^c$ are the auto terms and cross terms, respectively.

After scaling process and two-dimensional FT on the auto-correlation function, the LVD representation is obtained as

$$L_s(f, k) = \sum_{k=1}^{K} L_{sk}(f, k) = \sum_{k=1}^{K} A\delta(f - f_k)\delta(k - k_k) \tag{13}$$

where A is the amplitude, $\delta(\cdot)$ is Dirac delta function representing the LVD spread function along the representative axis f and k.

An example of LVD is given in Figure 2. The estimated carrier frequency and chirp rate of LFM signal are 50 Hz and 40 Hz/s respectively, which are the same as pre setted value.

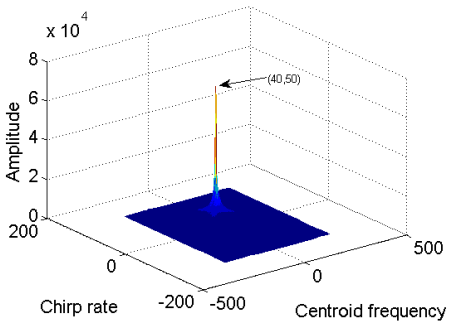

FIGURE 2. Stereogram of the LVD.

Now, the RR can be obtained through LVD by estimating the centroid frequency and chirp rate of a selected scatterer. To improve accuracy, we can utilize several scatterers for estimation and the average of these values is set as the optimal result of LVD.

C. ACCURATE SEARCH OF RR BASED ON GDM

Due to the interference of noise and other factors, the average RR is only a coarse estimation. Usually, the entropy function [23], [24] is invoked as an indication of ISAR image quality. When the entropy reaches the minimum, the quality of ISAR image is best. Hence, the accurate value of RR can be obtained by parameter search according to the image entropy principle.

Figure 3 illustrates image entropy versus the RR, which shows that the change of image entropy is a convex function. When the image entropy reaches the minimum, the corresponding RR is unique. Therefore, the parameter search of RR can be regarded as a convex optimization problem, GDM can be employed to search the global optimization [25]. The main process can be described as:

$$\xi_{t+1} = \xi_t + \Delta\xi \quad where\ \Delta\xi = -\eta\frac{\partial\psi}{\partial\xi} \tag{14}$$

where ψ is the object function, ξ is the variable and η is the search step length. According to Figure 3, it can be inferred that the iteration point can approach the global optimization point of the object function through several iterations.

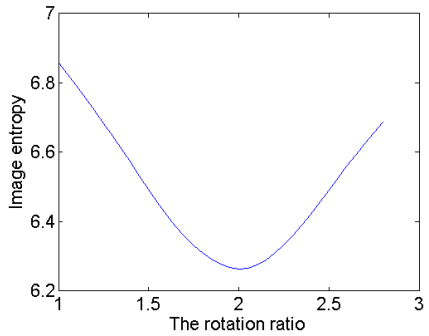

FIGURE 3. Image entropy versus the rotation ratio.

When the value meets that $|\Delta\psi| < \varepsilon$, the iteration comes to an end, where $\Delta\psi$ is the change of the object function between two adjacent iterations and ε is the threshold. Compared with the other searching methods like brute force search, the gradient descent method can obtain the global optimal solution quickly with low computational complexity.

The detail procedures of the new imaging method can be conducted as follows:

Step 1) Complete the range compression, the range alignment and the phase adjustment of the radar echoes;

Step 2) Extract the cross-range signal of the i-th (where $1 \leq i \leq N$ and N is the number of the range cells) range cell;

Step 3) Estimate the chirp rate and centroid frequency based on the LVD and obtain the coarse estimation of RR;

Step 4) Set the initial value as the coarse estimation got by step 3) and proper step length for the GDM and obtain the true value of RR via minimizing the image entropy;

Step 5) Compensate the quadratic phase terms by MFT and a well-focused image is got.

In summary, the procedures of the new ISAR imaging method are shown in Figure 4.

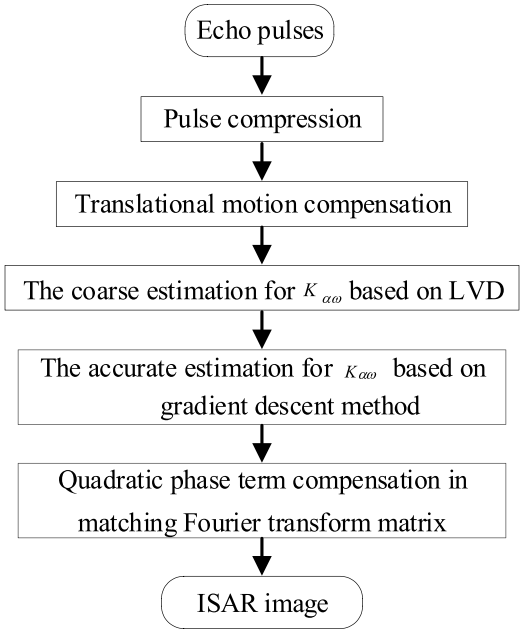

FIGURE 4. Flowchart of the proposed ISAR imaging method.

IV. SIMULATION RESULTS

In this section, we will confirm the validity and performance of the new imaging method with simulated data. Imaging results of precedent methods are provided as a comparison.

A. RESULTS OF SIMULATED AIRPLANE

The simulation parameter settings and motion parameters are illustrated in Table 1. The target scatterer model used in the simulation is an airplane contains 50 scatterers, as shown in Figure 5(a). The ISAR image obtained by the RD algorithm is shown in Figure 5(b). It is clear that the image is seriously blurred in the cross-range direction due to the time-varying Doppler frequency.

Now, the simulated data is applied to test the proposed method. Firstly, the signal in 98th range cell is selected and its parameter distribution got by LVD is shown in Figure 6 and the estimated RR is 1.70. To improve the accuracy, signals in four range cells are extracted to obtain an average value. The estimation results are shown in Table 2, from which we can see that the average RR is 2.08. Compared with the true

TABLE 1. Parameters of the radar system.

Parameter	Setting value
Carrier frequency	10GHz
Bandwidth	400MHz
Pulse width	50 μs
Complex sampling rate	50MHz
Pulse repeat frequency	400Hz
Pulse number	256
Initial angular velocity	0.04 rad/s
Angular acceleration	0.08 rad/s^2

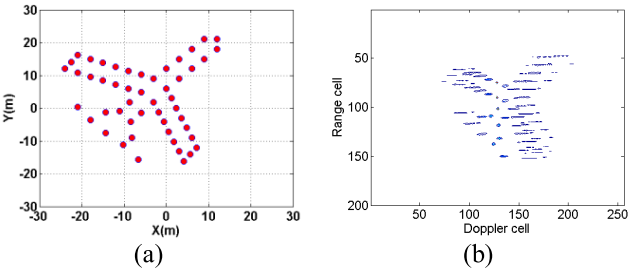

FIGURE 5. Simulated target model and RD image. (a) Target model; (b) RD image.

value of 2, the estimated one is inaccurate. Next, GDM is employed to search the optimal RR and imaging results. The initial value of RR is set as 2.08 and the search step length is set as 0.01. The threshold is set as the image entropy variation between two adjacent iterations is smaller than 10^{-6}. After 113 iterations, the iteration comes to an end. The image entropy versus the iteration number is shown in Figure 7(a). The searching result shows that the optimal value is 2, which

TABLE 2. Rotation ratio estimation based on LVD for different range cells.

Range cell	80th	85th	88th	98th	Average
$\tilde{k}_k$ (Hz/s)	49.38	25.59	19.72	-49.38	-
$\tilde{f}_k$ (Hz)	24.32	16.44	7.03	-29.04	-
$\tilde{K}_{\alpha\omega}$	2.03	1.80	2.80	1.70	2.08

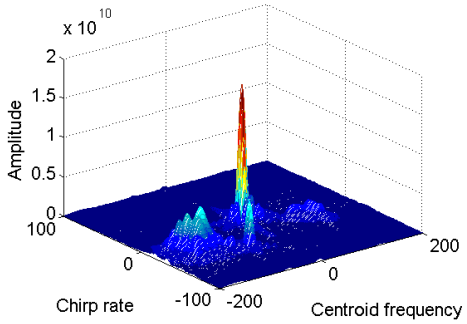

FIGURE 6. Parameter estimation of the LFM signal in 98th range cell.

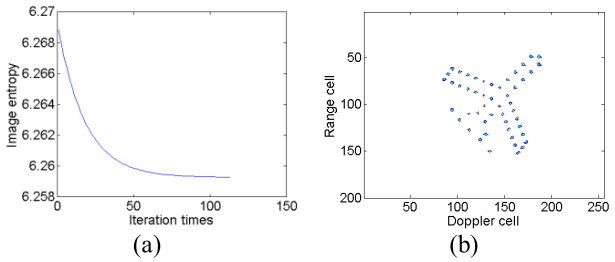

FIGURE 7. Searching for optimal RR and ISAR image through GDM. (a) entropy versus iteration times; (b) image obtained by MFT.

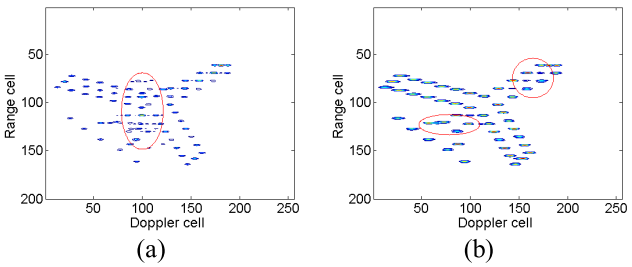

FIGURE 8. RID images. (a) WVD; (b) SPWVD.

agrees well with the real value. The optimal image is shown in Figure 7(b). Compared with Figure 5(b), the quality of the ISAR image in Figure 7(b) has been improved significantly.

RID images are obtained by taking the slices along the cross-range frequency domain and the method can form a series of images at different times. Next, RID images are utilized to compare with the image obtained by the proposed method. Figure 8(a) is the RID image produced by WVD. It can be noted that the image is smeared due to the significant cross-term interference. The RID image obtained by SPWVD

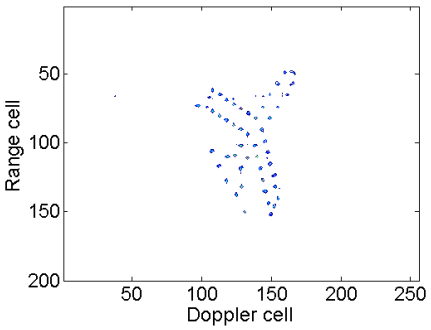

FIGURE 9. ISAR image based on LVD.

algorithm is illustrated in Figure 8(b), in which spurious scatterers exist in the red ellipse. Compared Figure 7(b) with Figure 8, it could be seen ISAR image in Figure 7(b) is well-focused in both range and cross-range directions and much better than RID images in Figure 8.

The parameter estimation imaging algorithm based on LVD is also provided to compare with the new imaging method. Given in Figure 9 is the final image. Although the image is well-focused, there are still some spurious scatterers that exist. Meanwhile, the imaging method requires estimating the parameters of all the LFM signals, which are computationally extensive and inefficient.

To evaluate the imaging results obtained by different algorithms, image entropies and contrasts are calculated, as listed in Table 3. The entropy of the image obtained by optimized MFT is minimum, which indicates that the effectiveness of the proposed method. However, the image contrasts indicate that the image quality got by SPWD method is the best. It can be seen that image entropy and contrast conflict with each other in this experiment. Hence, a more accurate indicator is needed to evaluate the ISAR image quality.

TABLE 3. Image entropies and contrasts of different methods.

Method	Figure	Entropy	Contrast
RD	Figure 5(b)	7.50	3.02
Optimized MFT	Figure 7(b)	6.26	4.12
WVD	Figure 8(a)	6.73	4.44
SPWVD	Figure 8(b)	6.33	6.84
LVD	Figure 9	6.30	4.10

Comparing the running time of these five methods listed in Table 4, it is seen that the running time of the new proposed imaging method is longer than that of RD and WVD, but shorter than that of SPWVD and LVD. Therefore, the proposed method is effective and efficient.

Next, the performance of RD, WVD and the proposed method is tested under different signal to noise (SNR) levels. The Gaussian white noise is added to the radar echoes and the SNR changes from 5dB to 15dB with a step length set as 1dB. 100 Monte Carlo simulations are performed to calculate the

TABLE 4. Computational complexity comparison of simulated data.

Method	Figure	Running time
RD	Figure 5(b)	0.11s
Optimized MFT	Figure 7(b)	18.32s
WVD	Figure 8(a)	3.59s
SPWVD	Figure 8(b)	31s
LVD	Figure 9	285.46s

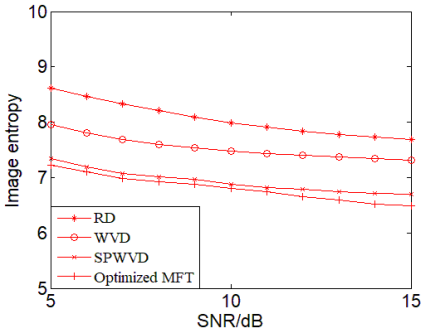

FIGURE 10. Average image entropy versus the SNR.

TABLE 5. Computational complexity comparison of boeing B727.

Method	Figure	Running time
RD	Figure 11(b)	0.12s
Optimized MFT	Figure 11(c)	23.88s
WVD	Figure 11(d)	1.93s
SPWVD	Figure 11(e)	10.58s
LVD	Figure 11(f)	144.32s

average entropy under each SNR and the result is illustrated in Figure 10. It can be seen that the proposed method performs best under different SNR. Therefore, it can be concluded that the proposed method is effective and efficient.

B. RESULTS OF BOEING B727

Next, the data of a Boeing B727 airplane provided by the U.S. Naval Research Laboratory [26] is applied to confirm the validity of the new imaging method. The data contains 256 successive pulses, where the carrier frequency is 9 GHz and the bandwidth are 150 MHz. Range compression and TMC have been already accomplished. Figure 11(a) and (b) show the high-resolution range profiles (HRRPs) and the corresponding RD image, respectively. It is clear that the image is seriously blurred in the cross-range direction due to the non-uniform rotating of the target.

When dealing with the data with the proposed method, the coarse estimation of RR based on LVD is 105.59. To obtain the accurate value of RR, the initial value of RR for GDM is set as 105.59, and the search step length is set as 1. The threshold is equal to the former experiment. After 208

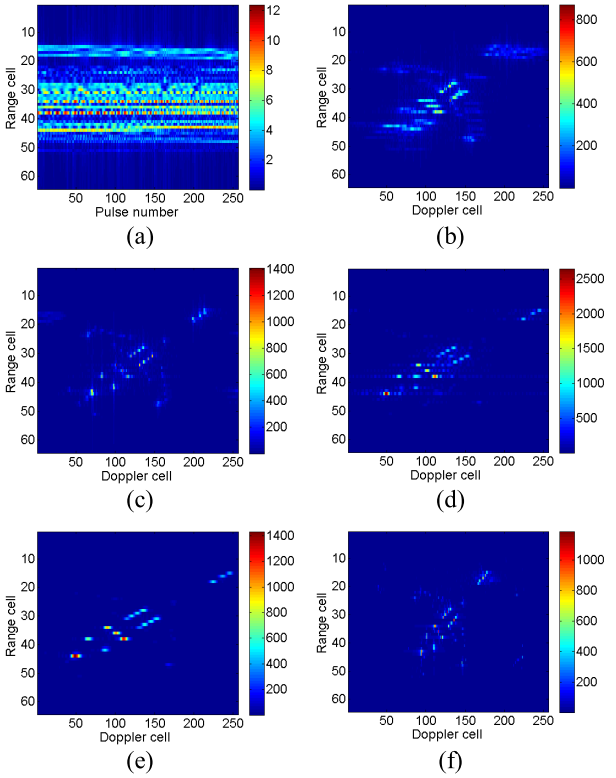

FIGURE 11. HRRPs and ISAR images. (a) HRRPs; (b) ISAR image based on RD. (c) ISAR image based on MFT; (d) ISAR image based on WVD; (e) ISAR image based on SPWVD; (f) ISAR image based on LVD.

iterations, the termination condition is met and the running results indicate that the optimal value of RR is 108.52. The optimal image is given in Figure 11(c). Comparing with Figure 11(b), the blurring is eliminated effectively.

Figure 11(d) is the RID image obtained by WVD algorithm. Due to the significant cross-term, the image is smeared severely. The image cannot provide much information of the target. Figure 11(e) shows the RID image based on SPWVD algorithm. Some weak scatterers especially in the wings and tail of the airplane lead to the loss of target shape information.

The ISAR image obtained by parameter estimation imaging method based on LVD is shown in Figure 11(f). Compared with Figure 11(c), it can be seen that the two-imaging method can almost reach the same imaging quality. However, the simulation times listed in Table 5 indicate that the former is inefficient. Considering the quality of the ISAR image and the computational complexity, we can conclude that the proposed method is more practical.

V. CONCLUSION

Focusing on the ISAR imaging of non-uniform rotating targets, a new imaging method based on optimized MFT is proposed in this paper. In the new method, the rotation of non-uniform rotating target after TMC is described by RR, which is the ratio of the chirp rate to the centroid frequency of LFM signal caused by scatterer. Using RR, the blurring caused by target's acceleration can be eliminated effectively

by MFT, and then a focused image can be obtained. Comparing with the classic imaging methods of non-uniform rotating targets, the imaging quality of the new method has been improved considerably. Moreover, the computational complexity is much lower than that of parameter estimation methods. Experimental analysis highlights the effectiveness and efficiency of the proposed method.

REFERENCES

[1] A. Lazarov and C. Minchev, "ISAR geometry, signal model, and image processing algorithms," *IET Radar, Sonar Navigat.*, vol. 11, no. 9, pp. 1425–1434, Sep. 2017.
[2] Y. Wang, A. Abdelkader, B. Zhao, and J. Wang, "ISAR imaging of maneuvering targets based on the modified discrete polynomial-phase transform," *Sensors*, vol. 15, no. 9, pp. 22401–22418, 2015.
[3] T. Itoh, H. Sueda, and Y. Watanabe, "Motion compensation for ISAR via centroid tracking," *IEEE Trans. Aerosp. Electron. Syst.*, vol. 32, no. 3, pp. 1191–1197, Jul. 1996.
[4] B. Tian, J. Zou, Z. Chen, and S. Xu, "Squint model interferometric ISAR imaging based on respective reference range selection and squint iteration improvement," *IET Radar, Sonar Navigat.*, vol. 9, no. 9, pp. 1366–1375, Dec. 2015.
[5] P. Hu, S. Xu, W. Wu, B. Tian, and Z. Chen, "IAA-based high-resolution ISAR imaging with small rotational angle," *IEEE Geosci. Remote Sens. Lett.*, vol. 14, no. 11, pp. 1978–1982, Nov. 2017.
[6] J. Zheng, H. Liu, Z. Liu, and Q. Liu, "ISAR imaging of ship targets based on an integrated cubic phase bilinear autocorrelation function," *Sensors*, vol. 17, no. 3, pp. 7276–7289, 2017.
[7] W. Wu, P. Hu, S. Xu, Z. Chen, and J. Chen, "Image registration for InISAR based on joint translational motion compensation," *IET Radar, Sonar Navigat.*, vol. 11, no. 10, pp. 1597–1603, Oct. 2017.
[8] B. Tian, Y. Liu, S. Xu, and Z. Chen, "Analysis of synchronization errors for InISAR on separated platforms," *IEEE Trans. Aerosp. Electron. Syst.*, vol. 52, no. 1, pp. 237–244, Feb. 2016.
[9] C.-C. Chen and H. Andrews, "Target-motion-induced radar imaging," *IEEE Trans. Aerosp. Electron. Syst.*, vol. AES-16, no. 1, pp. 2–14, Jan. 1980.
[10] V. C. Chen and W. J. Miceli, "Time-varying spectral analysis for radar imaging of manoeuvring targets," *IEE Proc.-Radar, Sonar Navigat.*, vol. 145, no. 5, pp. 262–268, Oct. 1998.
[11] G. Wang, "Inverse synthetic aperture radar imaging of nonuniformly rotating targets," *Opt. Eng.*, vol. 35, no. 10, pp. 3007–3011, Oct. 1996.
[12] Y. Wang, R. Xu, Q. Zhang, and B. Zhao, "ISAR imaging of maneuvering target based on the quadratic frequency modulated signal model with time-varying amplitude," *IEEE J. Sel. Topics Appl. Earth Observ. Remote Sens.*, vol. 10, no. 3, pp. 1012–1024, Mar. 2017.
[13] X. Lv, M. Xing, S. Zhang, and Z. Bao, "Keystone transformation of the Wigner–Ville distribution for analysis of multicomponent LFM signals," *Signal Process.*, vol. 89, no. 5, pp. 791–806, May 2009.
[14] R. Tao, B. Deng, and Y. Wang, "Research progress of the fractional Fourier transform in signal processing," *Sci. China. Inf. Sci.*, vol. 49, no. 1, pp. 1–25, Jan. 2006.
[15] X. Lv, G. Bi, C. Wan, and M. Xing, "Lv's distribution: Principle, implementation, properties, and performance," *IEEE Trans. Signal Process.*, vol. 59, no. 8, pp. 3576–3591, Aug. 2011.
[16] T. Thayaparan, W. Brinkman, and G. Lampropoulos, "Inverse synthetic aperture radar image focusing using fast adaptive joint time–frequency and three-dimensional motion detection on experimental radar data," *IET Signal Process.*, vol. 4, no. 4, pp. 382–394, Apr. 2010.
[17] Z. Bao, C. Sun, and M. Xing, "Time-frequency approaches to ISAR imaging of maneuvering targets and their limitations," *IEEE Trans. Aerosp. Electron. Syst.*, vol. 37, no. 3, pp. 1091–1099, Jul. 2001.
[18] W. Brinkman and T. Thayaparan, "Focusing inverse synthetic aperture radar images with higher-order motion error using the adaptive joint-time–frequency algorithm optimised with the genetic algorithm and the particle swarm optimisation algorithm—Comparison and results," *IET Signal Process.*, vol. 4, no. 4, pp. 329–342, 2010.
[19] Auger F. and Flandrin P. "Improving the readability of time-frequency and time-scaled representations by the reassignment method," *IEEE Trans. Signal Process.*, vol. 43, pp. 1068–1089, 1995.
[20] H. Ruan, Y. Wu, X. Jia, and W. Ye, "Novel ISAR imaging algorithm for maneuvering targets based on a modified keystone transform," *IEEE Geosci. Remote Sens. Lett.*, vol. 11, no. 1, pp. 128–132, Jan. 2014.
[21] Y. J. Huang, M. Cao, Y. W. Fu, Y. N. Li, and W. D. Jiang, "ISAR imaging of equably accelerative rotating targets based on matching Fourier transform," *J. Signal Process.*, vol. 25, no. 6, pp. 864–867, 2009.
[22] D. Li, X. Gui, H. Liu, J. Su, and H. Xiong, "An ISAR imaging algorithm for maneuvering targets with low SNR based on parameter estimation of multicomponent quadratic FM signals and nonuniform FFT," *IEEE J. Sel. Topics Appl. Earth Observ. Remote Sens.*, vol. 9, no. 12, pp. 5688–5702, Dec. 2016.
[23] X. H. Qiu, H. W. C. Alice, and S. Y. Yeo, "Fast minimum entropy phase compensation for ISAR imaging," *J. Electron. Inf. Technol.*, vol. 26, no. 10, pp. 1656–1660, Oct. 2004.
[24] L. Zhang, J.-L. Sheng, J. Duan, M.-D. Xing, Z.-J. Qiao, and Z. Bao, "Translational motion compensation for ISAR imaging under low SNR by minimum entropy," *EURASIP J. Adv. Signal Process.*, vol. 2013, no. 1, pp. 1–19, Dec. 2013.
[25] N. Jorge and S. Wright, *Numerical Optimization*. Springer, 2006, pp. 30–62.
[26] D. Li, H. Liu, X. Gui, and X. Zhang, "An efficient ISAR imaging method for maneuvering target based on synchrosqueezing transform," *IEEE Antennas Wireless Propag. Lett.*, vol. 15, pp. 1317–1320, 2016.

LEI ZUO was born in Heilongjiang, China, in 1981. He received the B.E. degree from Naval Aviation University, Yantai, China, and the M.E. and Ph.D. degrees from the Naval University of Engineering, Wuhan, China. He is currently a Lecturer with the College of Electronic Engineering, Naval University of Engineering. His major research interests are ISAR imaging and automation target recognition.

BINBIN WANG was born in Shanxi, China, in 1994. He received the B.E. degree from the South China University of Technology, Guangzhou, China, in 2016, and the M.E. degree from the National University of Defense Technology, Changsha, China, in 2018. He is currently pursuing the Ph.D. degree with the College of Electronic Engineering, Naval University of Engineering, Wuhan, China. His major research interests are ISAR imaging and radar signal processing.